Tsinghua Science and Technology
Doi: 10.26599/TST.2026.90100033

Research Article

RIS-Assisted Vehicular ISAC: A Robust Sensing-Centric System Design

Ruihang Yang, Li Wei(✉), Dezhi Wang, Bingzhe Du, Chen Zhu, Kai Wang, Zhengyu Zhu, Xiaoming Chen, Zhaohui Yang and Chongwen Huang(✉)

Abstract The convergence of sensing and communication, termed integrated sensing and communication (ISAC), is a cornerstone technology for next-generation autonomous vehicular networks. However, the performance of these systems is frequently constrained by harsh propagation environments featuring blockages. Reconfigurable intelligent surface (RIS) has emerged as a potent technique for intelligently tailoring the propagation environment, thereby yielding significant benefits for vehicular ISAC. This paper proposes a novel beamforming scheme integrating passive beamforming at RIS and active beamforming at vehicular ends. Efficient solutions to the formulated optimization problem are subsequently derived via alternating optimization (AO) and semidefinite relaxation (SDR) methods. Two practical criteria are employed for solving the optimization problem: one is fairness-oriented, i.e., ensuring uniform coverage, denoted as Max-Min-SNR; the other focuses on maximizing total information, termed Max-SIR. Simulation results show that, compared with existing baseline schemes, the Max-Min-SNR-based beamforming scheme attains a 7.66 dB (5.8-fold) enhancement in the minimum sensing SNR, while the Max-SIR-based scheme delivers a 45% information rate gain—thus verifying the superiority of the proposed beamforming scheme.

Keywords Integrated sensing and communication, reconfigurable intelligent surface, vehicular networks, sensing-centric design.

• Ruihang Yang, Bingzhe Du, Xiaoming Chen, Zhaohui Yang and Chongwen Huang are with College of Information Science & Electronic Engineering, Zhejiang University, Hangzhou 310027, (E-mails: {rhyang, dubingzhe, chen_xiaoming, yang_zhaohui, chongwenhuang}@zju.edu.cn).
• Li Wei is with School of Electrical and Electronics Engineering, Nanyang Technological University, Singapore 639798 (E-mail: lwei@ntu.edu.sg).
• Dezhi Wang is with QianYuan National Laboratory, Hangzhou 310024, China. (E-mail: dz_wang@zju.edu.cn).
• Chen Zhu is with Polytechnic Institute, Zhejiang University, Hangzhou 310027, China. (E-mail: zhuc@zju.edu.cn).
• Kai Wang is with Tianjin Industry and Information Techology Institute, Tianjin, 300374, China. (E-mail: 18622492083@163.com)
• Zhengyu Zhu is with the School of Electrical and Information Engineering, Zhengzhou University, Zhengzhou 450001, China. (E-mail: zhuzhengyu6@gmail.com).
Corresponding author: Chongwen Huang and Li Wei.
Manuscript received: 2025-11-25; revised: 2026-03-11; accepted: 2026-03-23

1 Introduction

The 6G wireless system is poised to revolutionize wireless communications by facilitating the sharing of time, space, and other multi-dimensional resources [1, 2]. Characterized by rapid data transfer, ultra-low latency, and reliable connectivity, 6G technology will lead to a new era of interconnected intelligence [3, 4]. This technological advancement is expected to significantly propel the development of intelligent transportation systems (ITS). As ITS rapidly evolves, the Internet of Vehicles (IoV) emerges as a pivotal component, interconnecting vehicles, infrastructure, pedestrians, and networks to enable real-time information exchange and processing [5], thereby significantly enhancing traffic efficiency and safety [6].

Despite the promising potential of IoV in intelligent transportation, several challenges and issues persist. The increasing number of vehicles and the exponential growth of data have put great pressure on the existing system architectures, impairing real-time data processing and transmission [7]. In ITS, real-time signal processing faces numerous challenges, including high data volume, low latency requirements, resource constraints, and dynamic environments [8]. Additionally, the rapidly changing nature of traffic conditions and environmental factors requires systems to quickly adapt and maintain situational awareness [9]. The rising vehicle interconnectivity further heightens the need for robust data security and privacy measures [10]. Addressing these challenges necessitates innovative solutions such as integrated sensing and communication (ISAC) [11, 12].

ISAC represents a cutting-edge system design approach that synergizes sensing technologies, computational power, and communication networks to develop systems that are more intelligent, efficient, and responsive [13, 14]. This integration facilitates real-time analytics, edge computation, and machine learning at the network's edge, propelling the development of future intelligent networks and constituting a critical advancement for IoV. In this context, ISAC is crucial

in enhancing vehicular operations, safety, and the overall driving experience [15]. The IoV ecosystem is rapidly evolving to meet the demands of autonomous driving, real-time traffic management, and enhanced infotainment services. ISAC aims to collect real-time data from the surroundings of vehicles [16, 17]. Furthermore, ISAC ensures accurate data capture for further processing and analysis, either on-board or via edge/cloud computation [11, 18]. ISAC also facilitates data exchange between vehicles, vehicles and infrastructure, pedestrians, and networks through wireless technologies such as Wi-Fi, 5G, and dedicated short-range communication (DSRC) [6, 19]. What's more, Positioning technology enhances real-time location tracking, environmental perception, and safety, supporting the cooperative behavior essential for the intelligent IoV ecosystem [20, 21]. Moreover, robust localization and cooperative sensing techniques are fundamental to the reliability of intelligent transportation systems, especially in complex environments where single-node observations are insufficient [22, 23]. Inspired by these cooperative paradigms, our robust ISAC framework seeks to guarantee reliable environmental perception even under stringent spatial and hardware constraints.

A pivotal technology within ISAC systems is beamforming, which enhances performance by directing signal energy toward specific targets, thereby improving communication quality and spectrum efficiency [24, 25]. Effective beamforming design is essential for optimizing the performance of ISAC in IoV contexts, where precise and reliable communication is paramount. However, designing beamforming strategies in ISAC systems presents significant challenges due to limited spectrum and energy resources, as well as the dynamic nature of vehicular environments [26]. Advanced resource allocation and optimization strategies are required to address these issues and ensure efficient beamforming. Authors in [27] have presented an ILSC framework to tackle the HFBS effect in ultra-massive MIMO for enhanced ISAC. The innovation in [28] develops a compressed sampling-based ISAC framework with a CU/RU architecture and OMP-SR algorithm for mmWave massive MIMO.

Reconfigurable intelligent surfaces (RIS) emerge as a promising solution to enhance beamforming in ISAC systems. An RIS typically consists of numerous passive reflecting elements whose phase shifts can be adjusted to control the direction of the reflected signals [29, 30]. Research shows that integrating RIS with emerging technologies can boost spectral efficiency [31], enhance physical layer security [32], and reduce interference [33]. Beyond acting as passive reflectors, RIS can function as transceivers, providing versatile communication capabilities, playing a crucial role in new applications and efficiencies [34, 35]. By dynamically controlling electromagnetic wave propagation, RIS significantly improves wireless communication performance, crucial for the IoV ecosystem [21, 36]. This manipulation enhances signal quality and reduces interference, ensuring reliable vehicle-to-everything (V2X) communication [37, 38]. In ISAC systems, RIS improves sensor accuracy and range by focusing electromagnetic waves and creating favorable propagation environments [39]. This enhancement allows precise data collection for better situational awareness [40]. RIS technology in the ISAC framework boosts computational and communication efficiency by reducing the need for retransmissions and error corrections [41], thereby decreasing computational load and enabling smoother operations [42].

While the cooperation between ISAC and RIS is still emerging, existing studies demonstrate the potential benefits of this integration. Research such as [43] has investigated joint design of constant-modulus waveforms and discrete RIS phase shifts to minimize user interference. Similarly, study in [26] has examined the application of RIS in boosting sensing capabilities and finding an optimal balance between communication efficiency and sensing accuracy. Additionally, authors in [44] have highlighted the advantages of integrating RIS and ISAC technologies, noting that RIS-controlled coupled channels in joint sensing and communication designs can significantly improve performance and power efficiency. In ISAC systems with IoV, beamforming design is further enhanced by RIS, which directs signal energy more effectively and mitigates the impact of blockages inherent in high-frequency millimeter-wave communications. RIS creates reliable virtual links between ISAC base stations and sensing targets, thereby enhancing overall system reliability and performance [26]. This integration is particularly transformative in urban environments, where buildings and other structures can obstruct or degrade signals [8, 17].

There are a lot of studies focusing on beamforming design for ISAC systems. The study in [18, 45] has explored the ISAC framework within Internet of Things (IoT) networks, focusing on optimizing power distribution for sensors and synthetic vectors to enhance signal clarity over background noise at the edge computation interface. Similarly, work in [46] has outlined an ISAC deployment strategy that combines mobile edge computation with sensor and communication systems through a repetitive matching algorithm for pairwise stability. Furthermore, work in [47] has set a threshold for sensed transmit power that, once reached, maintains constant data quality and introduces a unified ISAC resource allocation

problem aimed at maximizing convergence rates under various constraints. Additionally, authors in [48] have showcased a digital twin-powered network that leverages a multi-agent proximal policy optimization framework in ISAC, resulting in enhanced performance and energy efficiency. Content of [49] has introduced a vision-assisted beamforming framework for unmanned aerial vehicle (UAV)-to-vehicle communications, leveraging YOLOv5 for vehicle detection and a Sage-Husa filter for tracking, to optimize beamforming and reduce communication overhead. Achievements in [50] have explored UAV-aided ISAC with mobile edge computation (MEC) for target recognition, employing an efficient algorithm to minimize system cost by optimizing sensing scheduling, power, and UAV trajectory, despite the nonconvexity of the problem. Research in [51] has introduced sensing-assisted beamforming for vehicles on complex roads using ISAC and a curvilinear coordinate system within an interacting multiple model - extended Kalman filter (IMM-EKF) framework, aiming to enhance tracking accuracy and quality of service (QoS) by optimizing array size and beam width. [52] maximize radar SINR by jointly optimizing the DFRC BS beamforming and active RIS coefficients under UE QoS and transmit power constraints.

Combining RIS with ISAC beamforming enhances signal coverage, strength, and quality by dynamically controlling signal reflections, improving energy efficiency, and managing interference. This integration supports better environmental sensing, optimizes resource, and facilitates multi-user communication, making it essential for advancing future smart communication systems. Previous studies have efficiently integrated sensing, computation, and communication functions within the ISAC framework. However, ISAC faces significant challenges such as limited spectrum and energy resources, complexities in interference management, and high demands for real-time data processing. Additionally, the inherent complexity and non-convexity of related optimization problems, along with signal attenuation, path loss, and the need for multi-functional integration and coordination, further complicate these tasks. Moreover, the inclusion of RIS introduces additional layers of complexity and opportunity, necessitating advanced strategies for their effective integration into ISAC systems. More importantly, a critical limitation persists in the current literature: the overwhelming majority of these works predominantly adopt a communication-centric philosophy (treating sensing merely as a secondary constraint) or focus on optimizing the average or sum sensing performance.

This leads to a fundamental question: how should the system behave when faced with a choice between slightly improving communication throughput and ensuring that a potential hazard at the edge of the sensing area is reliably detected?

The existing body of work, while impressive, leaves a critical gap for safety-driven vehicular applications. In autonomous driving, ensuring robust and reliable sensing is non-negotiable and must often take precedence over maximizing communication throughput. Designs based on a balanced trade-off or a communication-first objective may fail in critical scenarios, as even a single "weak spot" in the sensing coverage could be catastrophic.

The principle of robust design, which focuses on optimizing worst-case spatial performance rather than the average, is therefore paramount. In this context, the term "robust" embodies a dual design philosophy: (1) spatial robustness, which ensures uniform safety-critical sensing coverage over a predictive area by optimizing the worst-case performance, thereby eliminating perceptual blind spots; and (2) imperfection robustness, which guarantees reliable ISAC performance even under severe channel estimation errors and hardware limitations.

Motivated by this, our work departs from conventional designs and proposes two distinct, sensing-centric robust design philosophies, each realized as a novel joint beamforming algorithm. In this context, the term "robust" embodies a dual design philosophy: (1) spatial robustness, which ensures uniform safety-critical sensing coverage over a predictive area by optimizing the worst-case performance, thereby eliminating perceptual blind spots; and (2) imperfection robustness, which guarantees reliable ISAC performance even under severe channel estimation errors and hardware limitations. We directly address the challenge of providing guaranteed sensing performance in a dynamic, behavior-aware manner. The main contributions of this paper are:

1. **Two Novel Sensing-Centric Formulations and Algorithms:** We propose and formulate two new joint active and passive beamforming algorithms, each addressing a different facet of sensing excellence. One is robust Max-Min-SNR. Its core contribution is ensuring uniform and reliable sensing coverage by maximizing the worst-case performance, directly addressing the safety requirement of eliminating perceptual blind spots. The other is information-theoretic Max-SIR. Its contribution lies in providing a design that optimizes the total amount of information gathered from the environment, offering a different, information-driven approach to enhancing overall situational awareness. For both non-convex problems, we develop efficient iterative solutions based on

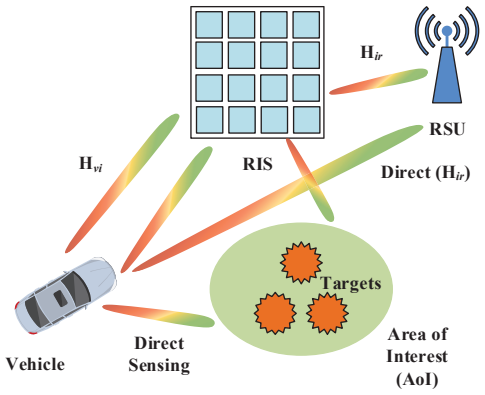

Fig. 1 System model of the proposed RIS-assisted vehicular ISAC system.

alternating optimization (AO) and semidefinite relaxation (SDR).

2. **Quantified Performance Superiority:** We provide extensive simulation results that quantify the significant performance gains of our proposed criteria. Our Max-Min-SNR design is shown to be highly effective for robust coverage. It achieves a remarkable 7.66 dB improvement in worst-case sensing SNR over a system without an RIS and can support up to 59% higher communication data rates than traditional decoupled optimization for the same stringent sensing requirement. Our Max-SIR design proves to be a powerful alternative focused on overall perception. It achieves a total sensing information rate that is 45% higher than the weighted sum optimization baseline.

The remainder of this paper is organized as follows. Section 2 details the system model. Section 3 presents the problem formulation and the proposed algorithm. Section 4 reveals the simulation results. Section 5 concludes the paper.

2 System Model

2.1 System Scenario

The scenario under consideration involves a vehicle, a RIS, a roadside unit (RSU), and sensing targets within the vehicle's environment. We display this scenario in Fig. 1. The components are listed respectively:

- **Vehicle:** The vehicle is equipped with a uniform linear array (ULA) of N_t antennas with inter-element spacing d_t. It acts as the ISAC transmitter.
- **RIS:** An RIS, comprising a ULA of N passive reflecting elements with spacing d_{ris}, is deployed in the environment (e.g., on a building facade) to assist the vehicle.
- **RSU:** The RSU, acting as the communication destination, is equipped with a ULA of N_r antennas.
- **Area of Interest (AoI):** Using a kinematic bicycle model [21], the vehicle predicts its immediate trajectory, defining a dynamic AoI. This continuous area is discretized into M critical monitoring points, $\mathcal{S}_{\text{AoI}} = \{(\theta_m, r_m)\}_{m=1}^{M}$, for tractable optimization.

For better comprehension, we abstract the concepts in the system diagram and draw them into an easy-to-read schematic diagram in Fig. 2

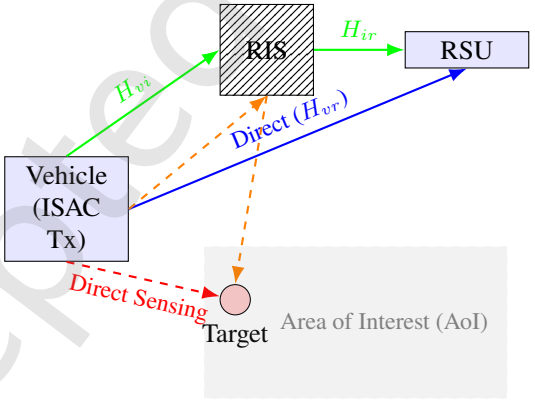

Fig. 2 Abstract schematic diagram of system model.

2.2 Behavior-Aware AoI Prediction Based on Kinematic Motion

A fundamental aspect of our intelligent vehicular system is its ability to proactively sense the environment where it is most likely to encounter critical events. To achieve this, we define a dynamic AoI based on the vehicle's predicted behavior. This proactive AoI definition is crucial as it guides the subsequent joint design of the active beamforming at the vehicle and the passive beamforming at the RIS to ensure that sensing resources are intelligently allocated.

We leverage a standard kinematic bicycle model to forecast the vehicle's immediate future motion [21]. From Fig. 3, the model provides a reliable relationship between the vehicle's control inputs and its physical trajectory. The key parameters governing the motion are the vehicle's current longitudinal velocity v, its acceleration a, and the steering angle ϕ of its front wheels.

Assuming these control inputs remain constant over a short prediction horizon Δt, the vehicle's motion can be accurately approximated as a circular arc. The vehicle's future positions $(d_x(t), d_y(t))$ for $t \in [t_0, t_0 + \Delta t]$ can be determined by integrating the following set of differential equations:

$$\dot{d_x}(t) = (v_0 + a(t - t_0)) \cos(\vartheta(t)) \tag{1}$$

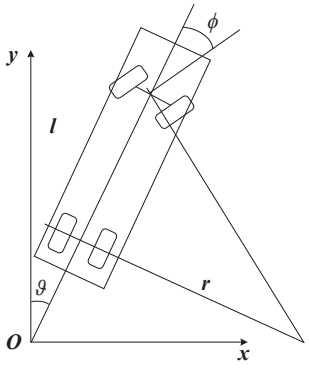

Fig. 3 Kinematic model of vehicle referring to the bicycle model.

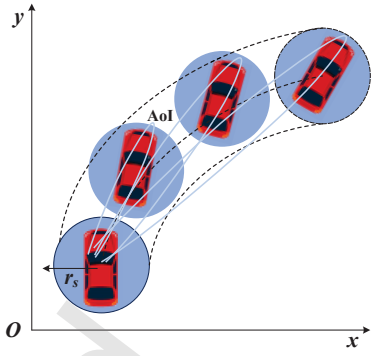

Fig. 4 AoI prediction based on the real-time behaviors and the state of the vehicle.

$$\dot{d}_y(t) = (v_0 + a(t - t_0))\sin(\vartheta(t)) \tag{2}$$

$$\dot{\vartheta}(t) = \frac{(v_0 + a(t - t_0))\tan(\phi)}{l} \tag{3}$$

where v_0 and ϑ_0 are the velocity and heading angle at the initial time t_0, and l is the vehicle's wheelbase. Solving these equations yields a predicted path, which represents the most probable trajectory of the vehicle in the near future.

The predicted trajectory alone is insufficient; a safety-critical system must be aware of the space around the vehicle. Therefore, we define the AoI as the region swept by a "safety bubble" of radius r_s as it moves along the predicted path centerline. This creates a corridor-like area that encompasses the vehicle's future occupied space and its immediate surroundings, as illustrated in Fig. 4. This behavior-aware AoI is not static but dynamically adapts in real-time to the driver's actions (or the autonomous controller's decisions). For instance, a larger steering angle will result in a curved AoI, prompting the ISAC system to allocate sensing resources towards the inside of the turn.

In highly dynamic vehicular environments, rapid changes in network topology pose a significant challenge for real-time channel state information (CSI) acquisition and RIS configuration, often leading to the "outdated CSI" problem. However, our proposed framework enhances robustness against such delays. By defining a predictive spatial "safety bubble" (AoI) rather than tracking a single instantaneous point, and by optimizing for the worst-case performance across this entire area, the system guarantees that targets remain within a reliable high-SNR monitoring zone even if they undergo unpredictable micro-movements during the configuration delay. Future work will focus on integrating predictive beamforming and real-time channel tracking techniques to further mitigate the performance degradation caused by outdated CSI in ultra-high-speed scenarios.

For the purpose of formulating a tractable optimization problem, we discretize this continuous AoI. We sample a set of M critical monitoring points, $\mathcal{S}_{\text{AoI}} = \{(\theta_m, r_m)\}_{m=1}^{M}$, that effectively represent the entire region.

This discretized set $\mathcal{S}_{\text{AoI}} = \{(\theta_m, r_m)\}_{m=1}^{M}$ provides the concrete target coordinates for the sensing performance constraints in our subsequent problem formulations (e.g., Eq. 10b). Note that the distance r_m directly dictates the value of the target-specific parameter β_m in the sensing channel model, ensuring that distance-dependent path loss is fully accounted for in the beamforming optimization.

It is worth noting that the accuracy of the kinematic bicycle model is sensitive to vehicle speed. In high-speed scenarios, the trajectory prediction error naturally increases. However, our proposed robust design effectively mitigates this uncertainty. By dynamically enlarging the radius of the safety bubble r_s to encapsulate the increased prediction variance, the spatial Max-Min optimization guarantees that even if the vehicle or target deviates significantly within this expanded bubble, it will still be reliably illuminated and detected.

2.3 Signal Model

The vehicle generates a baseband signal vector $\mathbf{s}(t) \in \mathbb{C}^{N_s \times 1}$ for N_s data streams, satisfying the normalization $\mathbb{E}[\mathbf{s}(t)\mathbf{s}^H(t)] = \mathbf{I}_{N_s}$. This signal is precoded by an active beamforming matrix $\mathbf{F}_D \in \mathbb{C}^{N_t \times N_s}$. The transmitted signal is $\mathbf{x}(t) = \mathbf{F}_D\mathbf{s}(t)$. The spatial distribution of the transmitted power is fully characterized by the transmit covariance matrix:

$$\mathbf{R}_D = \mathbb{E}[\mathbf{x}(t)\mathbf{x}^H(t)] = \mathbf{F}_D\mathbf{F}_D^H \tag{4}$$

This matrix must be positive semidefinite ($\mathbf{R}_D \succeq 0$) and adhere to the total power constraint, $\text{Tr}(\mathbf{R}_D) = P_{\text{total}}$.

The RIS introduces controllable, reflected signal paths, which must be mathematically modeled.

The RIS's response is modeled by a diagonal phase-shift

matrix $\mathbf{\Phi} \in \mathbb{C}^{N\times N}$, defined as:

$$\mathbf{\Phi} = \text{diag}(e^{j\phi_1}, \ldots, e^{j\phi_N}) = \text{diag}(\mathbf{v}) \tag{5}$$

where $\mathbf{v} = [e^{j\phi_1}, \ldots, e^{j\phi_N}]^T$ is the vector of reflection coefficients, and $\phi_n \in [0, 2\pi)$ is the controllable phase shift of the n-th element. Each element is subject to the unit-modulus constraint $|v_n| = 1$.

The signal from the vehicle to the RSU propagates through two paths: a direct link and an RIS-reflected link. We assume all channels are known, obtainable via advanced CSI estimation techniques [53]. The direct Vehicle-to-RSU channel, Vehicle-to-RIS channel, and RIS-to-RSU channel are denoted as $\mathbf{H}_{vr} \in \mathbb{C}^{N_r\times N_t}$, $\mathbf{H}_{vi} \in \mathbb{C}^{N\times N_t}$, and $\mathbf{H}_{ir} \in \mathbb{C}^{N_r\times N}$, respectively. These channels are modeled as Rician fading channels, composed of both line-of-sight (LoS) and non-line-of-sight (NLoS) components, which is suitable for typical urban deployments. The signal arriving at the RSU via the RIS experiences a cascaded channel path $\mathbf{H}_{ir}\mathbf{\Phi}\mathbf{H}_{vi}$. Thus, the total effective end-to-end communication channel is the coherent sum of these two paths:

$$\mathbf{H}_{\text{eff}}(\mathbf{v}) = \underbrace{\mathbf{H}_{vr}}_{\text{Direct Path}} + \underbrace{\mathbf{H}_{ir}\text{diag}(\mathbf{v})\mathbf{H}_{vi}}_{\text{RIS-Reflected Path}} \tag{6}$$

The received communication signal is $\mathbf{y}_c(t) = \mathbf{H}_{\text{eff}}(\mathbf{v})\mathbf{x}(t) + \mathbf{n}_c(t)$, where $\mathbf{n}_c(t) \sim \mathcal{CN}(0, \sigma_c^2\mathbf{I}_{N_r})$ is the receiver noise.

The achievable communication rate is given by the Shannon capacity formula for the effective MIMO channel:

$$R_{\text{comm}}(\mathbf{R}_D, \mathbf{v}) = \log_2 \det\left(\mathbf{I}_{N_r} + \frac{1}{\sigma_c^2}\mathbf{H}_{\text{eff}}(\mathbf{v})\mathbf{R}_D\mathbf{H}_{\text{eff}}^H(\mathbf{v})\right) \tag{7}$$

This metric quantifies the maximum error-free data throughput. We will impose a minimum QoS constraint, $R_{\text{comm}} \geqslant \Gamma_{\min}$.

For sensing, the echo from a target at (θ_m, r_m) also returns to the vehicle via both direct and RIS-reflected paths.

- **Vehicle-Target-Vehicle** (Direct Echo): The signal travels from the vehicle to the target and reflects back. The round-trip steering vector for this path is $\mathbf{a}_t(\theta_m)$.
- **Vehicle-RIS-Target-RIS-Vehicle** (Reflected Echo): This is a more complex path. The signal goes from the vehicle to the RIS, reflects towards the target, reflects off the target back to the RIS, and finally reflects from the RIS back to the vehicle.

To formulate a tractable model, we focus on the coherent combination of the signals arriving at the vehicle's receiver. The effective channel response that shapes the transmitted covariance matrix $\mathbf{R}_D$ for sensing in direction θ_m is determined by the "virtual" steering vector that includes the RIS path. The signal arriving at the target from the vehicle and RIS can be modeled by an effective transmit steering vector:

$$\tilde{\mathbf{a}}_{\text{tx}}(\mathbf{v}, \theta_m) = \mathbf{a}_t(\theta_m) + \mathbf{H}_{vi}^H\text{diag}(\mathbf{v})^H\mathbf{a}_r(\theta_m) \tag{8}$$

This vector describes the coherent superposition of the direct wave and the RIS-reflected wave at the target's location. The power impinging on the target is proportional to $||\tilde{\mathbf{a}}_{\text{tx}}(\mathbf{v}, \theta_m)||^2$. Assuming a similar round-trip path for the echo, the received sensing signal power at the vehicle is determined by the matrix $\mathbf{A}(\mathbf{v}, \theta_m) = \tilde{\mathbf{a}}_{\text{tx}}(\mathbf{v}, \theta_m)\tilde{\mathbf{a}}_{\text{tx}}^H(\mathbf{v}, \theta_m)$.

Under the far-field approximation, the target is sufficiently distant such that the transmit and receive angles relative to the vehicle and RIS can be approximated by a unified angle θ_m. The total transmit power projected towards this virtual direction is given by $\text{Tr}(\mathbf{R}_D\mathbf{A}(\mathbf{v}, \theta_m))$. Consequently, the received sensing echo power is directly proportional to this term. Furthermore, β_m is a target-specific parameter that lumps together fixed antenna gains, radar cross-section (RCS), and the variable two-way path loss (which is determined by the specific distance r_m).

The received SNR for a target at (θ_m, r_m) is the ratio of the echo signal power to the noise power at the vehicle's receiver. Based on the radar equation and the effective sensing channel model, the SNR can be expressed as:

$$\text{SNR}_{\text{sense}}(\mathbf{R}_D, \mathbf{v}, \theta_m) = \frac{\beta_m}{\sigma_s^2}\text{Tr}(\mathbf{R}_D\mathbf{A}(\mathbf{v}, \theta_m)) \tag{9}$$

where σ_s^2 is the sensing receiver noise variance, and β_m is a constant that lumps together fixed parameters like the two-way path loss (proportional to $1/r_m^4$), target radar cross-section (RCS), and antenna gains. The term $\text{Tr}(\mathbf{R}_D\mathbf{A}(\mathbf{v}, \theta_m))$ represents the total power directed towards and received from the virtual direction defined by the direct and RIS-reflected paths. This metric is crucial as higher SNR leads directly to better detection probability and estimation accuracy.

3 Problem Formulation and Proposed Algorithms

Based on the detailed system model, we now formulate two distinct, sensing-centric optimization problems for the joint design of the active covariance matrix $\mathbf{R}_D$ and the passive phase-shift vector $\mathbf{v}$. Each formulation represents a different philosophy for achieving robust sensing performance. We present each design in a separate subsection, complete with its mathematical formulation, a step-by-step solution methodology, and a computational complexity analysis.

3.1 Design I: Robust Beamforming via Max-Min Sensing SNR

The primary goal of this design is to ensure a uniform and reliable sensing capability across the entire AoI. This is critical

for safety, as it prevents the existence of "weak spots" where a target might be missed. We achieve this by maximizing the minimum (i.e., worst-case) sensing SNR among all critical monitoring points.

3.1.1 Problem Formulation

Let τ be an auxiliary variable representing the minimum sensing SNR as the SNR expression is complicated. Our objective is to maximize τ for the constraint in (10b). The problem can be formulated as:

$$\max_{\mathbf{R}_D,\mathbf{v},\tau} \quad \tau \tag{10a}$$

$$\text{s.t.} \quad \text{SNR}_{\text{sense}}(\mathbf{R}_D,\mathbf{v},\theta_m) \geqslant \tau, \quad \forall m \in \{1,...,M\} \tag{10b}$$

$$R_{\text{comm}}(\mathbf{R}_D,\mathbf{v}) \geqslant \Gamma_{\min} \tag{10c}$$

$$\text{Tr}(\mathbf{R}_D) = P_{\text{total}}, \quad \mathbf{R}_D \succeq 0 \tag{10d}$$

$$|v_n| = 1, \quad \forall n \in \{1,...,N\} \tag{10e}$$

Substituting the expressions for SNR and rate from (7) and (9), we get:

$$\max_{\mathbf{R}_D,\mathbf{v},\tau} \quad \tau \tag{11a}$$

$$\text{s.t.} \quad \frac{\beta_m}{\sigma_s^2}\text{Tr}(\mathbf{R}_D\mathbf{A}(\mathbf{v},\theta_m)) \geqslant \tau, \quad \forall m \in \{1,...,M\} \tag{11b}$$

$$\log_2\det\left(\mathbf{I}_{N_r} + \frac{1}{\sigma_c^2}\mathbf{H}_{\text{eff}}(\mathbf{v})\mathbf{R}_D\mathbf{H}_{\text{eff}}^H(\mathbf{v})\right) \geqslant \Gamma_{\min} \tag{11c}$$

$$\text{Tr}(\mathbf{R}_D) = P_{\text{total}}, \quad \mathbf{R}_D \succeq 0 \tag{11d}$$

$$|v_n| = 1, \quad \forall n \in \{1,...,N\} \tag{11e}$$

This problem is highly non-convex due to the coupling of $\mathbf{R}_D$ and $\mathbf{v}$ in the constraints (11b) and (11c), and the non-convex unit-modulus constraint (10e).

To find a high-quality solution, we propose an iterative algorithm based on AO, which decouples the problem by optimizing one variable while keeping the other fixed.

Sub-problem 1 (Optimizing Active Beamforming $\mathbf{R}_D$) : With a fixed RIS phase-shift vector $\mathbf{v}$, the effective channels $\mathbf{H}_{\text{eff}}(\mathbf{v})$ and the sensing matrices $\mathbf{A}(\mathbf{v},\theta_m)$ become constants. The problem for optimizing $\mathbf{R}_D$ is:

$$\max_{\mathbf{R}_D,\tau} \quad \tau \tag{12a}$$

$$\text{s.t.} \quad \text{Tr}(\mathbf{R}_D\mathbf{A}(\mathbf{v},\theta_m)) \geqslant \tau\frac{\sigma_s^2}{\beta_m}, \quad \forall m \tag{12b}$$

$$\log_2\det\left(\mathbf{I} + \frac{1}{\sigma_c^2}\mathbf{H}_{\text{eff}}\mathbf{R}_D\mathbf{H}_{\text{eff}}^H\right) \geqslant \Gamma_{\min} \tag{12c}$$

$$\text{Tr}(\mathbf{R}_D) = P_{\text{total}}, \quad \mathbf{R}_D \succeq 0 \tag{12d}$$

This is a convex optimization problem. The objective is linear. The sensing constraints are linear matrix inequalities (LMIs). The communication constraint is convex since $\log\det(\cdot)$ is a concave function. Therefore, this is a standard semidefinite program (SDP) that can be solved efficiently to global optimality using interior-point methods, for instance, with solvers like CVX [54].

Once the optimal transmit covariance matrix $\mathbf{R}_D^*$ is obtained, the actual active precoding matrix $\mathbf{F}_D^*$ can be extracted via matrix decomposition techniques. Specifically, if the rank constraint $\text{rank}(\mathbf{R}_D^*) \leqslant N_s$ is satisfied, $\mathbf{F}_D^*$ can be directly recovered using eigenvalue decomposition (EVD). If the rank exceeds N_s due to the SDP relaxation, standard Gaussian randomization or eigenvalue truncation techniques can be employed to generate a high-quality feasible $\mathbf{F}_D^*$.

Sub-problem 2 (Optimizing Passive Beamforming $\mathbf{v}$) : With a fixed active covariance $\mathbf{R}_D$, the problem for $\mathbf{v}$ is still non-convex due to the unit-modulus constraint. We employ semidefinite relaxation (SDR) [55] to find a solution. First, we need to express the constraints as quadratic forms of $\mathbf{v}$. The effective channel is $\mathbf{H}_{\text{eff}}(\mathbf{v}) = \mathbf{H}_{vr} + \mathbf{H}_{ir}\text{diag}(\mathbf{H}_{vi}\mathbf{x}) = \mathbf{H}_{vr} + \sum_n v_n\mathbf{h}_{ir,n}\mathbf{h}_{vi,n}^T$, which is complex. The rate constraint is difficult to handle directly. A common approach is to work with a more tractable lower bound, such as the minimum mean square error (MMSE) relationship. For the sensing SNR, we expand $\mathbf{A}(\mathbf{v},\theta_m)$:

$$\begin{aligned}\mathbf{A}(\mathbf{v},\theta_m) &= (\mathbf{a}_t + \mathbf{G}^H\mathbf{v}^*)(\mathbf{a}_t^H + \mathbf{v}^T\mathbf{G}) \\ &= \mathbf{a}_t\mathbf{a}_t^H + \mathbf{a}_t\mathbf{v}^T\mathbf{G} + \mathbf{G}^H\mathbf{v}^*\mathbf{a}_t^H + \mathbf{G}^H\mathbf{v}^*\mathbf{v}^T\mathbf{G}\end{aligned} \tag{13}$$

where we use simplified notation $\mathbf{a}_t = \mathbf{a}_t(\theta_m)$ and $\mathbf{G} = \text{diag}(\mathbf{a}_r(\theta_m))\mathbf{H}_{vi}$. The term $\text{Tr}(\mathbf{R}_D\mathbf{A}(\mathbf{v},\theta_m))$ becomes a quadratic function of $\mathbf{v}$. Let $\bar{\mathbf{v}} = [\mathbf{v}^T, 1]^T$ and define $\mathbf{V} = \bar{\mathbf{v}}\bar{\mathbf{v}}^H$. This matrix must satisfy $\mathbf{V} \succeq 0$, $\text{diag}(\mathbf{V}) = \mathbf{1}$, and the (relaxed) rank-one constraint $\text{rank}(\mathbf{V}) = 1$. All quadratic terms in $\mathbf{v}$ can be rewritten as linear traces involving $\mathbf{V}$. For example, $\mathbf{v}^T\mathbf{Q}\mathbf{v}^* = \text{Tr}(\mathbf{Q}\mathbf{v}^*\mathbf{v}^T) = \text{Tr}(\mathbf{Q}\mathbf{V}_{1:N,1:N})$. The problem is then transformed into an SDP over the variable $\mathbf{V}$, by dropping the rank-one constraint.

$$\max_{\mathbf{V},\tau} \quad \tau \tag{14a}$$

$$\text{s.t.} \quad \mathbf{V}_{n,n} = 1, \quad \forall n \in \{1,...,N+1\} \tag{14b}$$

$$\mathbf{V} \succeq 0 \tag{14c}$$

After solving this SDP for $\mathbf{V}^*$, if it is not rank-one, Gaussian randomization is used to extract a high-quality feasible vector $\mathbf{v}$.

3.1.2 *Algorithm and Complexity Analysis*

The overall algorithm iterates between solving these two sub-problems.

Algorithm 1 Alternating Optimization for Max-Min-SNR ISAC

Initialize:
Channel Matrices $\{\mathbf{H}_{vr}, \mathbf{H}_{vi}, \mathbf{H}_{ir}\}$, QoS $\Gamma_{\min}$, Power P_{total}, Tolerance ϵ, $K_{\max}$.
$k \leftarrow 0$, $\tau^{(0)} \leftarrow 0$.
Generate $\mathbf{v}^{(0)}$ such that $|v_n^{(0)}| = 1, \forall n$.
Predict and discretize AoI into $\mathcal{S}_{\text{AoI}}$.
repeat
  Step 1: Update Active Beamforming $\mathbf{R}_D$
  Solve the convex problem (12) with fixed $\mathbf{v} \leftarrow \mathbf{v}^{(k)}$ to obtain $\mathbf{R}_D^{(k+1)}$ and $\tau^{(k+1/2)}$.
  Step 2: Update Passive Beamforming $\mathbf{v}$
  Solve the non-convex problem for $\mathbf{v}$ with fixed $\mathbf{R}_D \leftarrow \mathbf{R}_D^{(k+1)}$ via SDR to obtain $\mathbf{v}^{(k+1)}$ and $\tau^{(k+1)}$.
  Step 3: Update Iteration Index
  $k \leftarrow k + 1$.
until $|\tau^{(k)} - \tau^{(k-1)}|/\tau^{(k-1)} \leqslant \epsilon$ **or** $k \geqslant K_{\max}$.
return $\mathbf{R}_D^* \leftarrow \mathbf{R}_D^{(k)}$ and $\mathbf{v}^* \leftarrow \mathbf{v}^{(k)}$.

The computational complexity of Algorithm 1 is dominated by solving the two SDP sub-problems within each AO iteration. Let I_{AO} denote the number of iterations for convergence.

- **Sub-problem 1 (Optimizing $\mathbf{R}_D$):** The complexity of solving the SDP for the $N_t \times N_t$ active covariance matrix is approximately $\mathcal{O}(MN_t^3)$, where M is the number of monitoring points.
- **Sub-problem 2 (Optimizing $\mathbf{v}$ via SDR):** The complexity of solving the SDR for the $(N+1) \times (N+1)$ passive beamforming matrix is dominated by the number of RIS elements N, scaling as $\mathcal{O}(N^4)$.

Therefore, the overall complexity of the proposed algorithm is given by $\mathcal{O}\left(I_{AO} \cdot \left(MN_t^3 + N^4\right)\right)$.

3.2 Design II: Information-Theoretic Beamforming via SIR Maximization

This design adopts an information-theoretic lens, aiming to maximize the total amount of information extracted from the sensing environment, ensuring a rich perceptual understanding.

3.2.1 *Problem Formulation*

The objective is to maximize the weighted sum of Sensing Information Rate (SIR) across the AoI, subject to both sensing and communication QoS constraints.

$$\max_{\mathbf{R}_D, \mathbf{v}} \quad \sum_{m=1}^{M} w_m \cdot R_{\text{sense}}(\mathbf{R}_D, \mathbf{v}, \theta_m) \tag{15a}$$

$$\text{s.t.} \quad R_{\text{sense}}(\mathbf{R}_D, \mathbf{v}, \theta_m) \geqslant S_{\min}, \forall m \in \{1, ..., M\} \tag{15b}$$

$$R_{\text{comm}}(\mathbf{R}_D, \mathbf{v}) \geqslant \Gamma_{\min} \tag{15c}$$

$$\text{Tr}(\mathbf{R}_D) = P_{\text{total}}, \quad \mathbf{R}_D \succeq 0 \tag{15d}$$

$$|v_n| = 1, \quad \forall n \in \{1, ..., N\} \tag{15e}$$

where $\{w_m\}$ are non-negative weights reflecting the importance of each monitoring point, and $S_{\min}$ is a minimum required SIR for fairness. This problem is also non-convex for the same reasons as the Max-Min-SNR problem.

We again use AO. The logic is similar, but the objective and constraints change.

Sub-problem 1 (Optimizing Active Beamforming $\mathbf{R}_D$) : For a fixed $\mathbf{v}$, the problem becomes:

$$\max_{\mathbf{R}_D} \quad \sum_{m=1}^{M} w_m \cdot \log_2(1 + \kappa_m \cdot \text{Tr}(\mathbf{R}_D \mathbf{A}(\mathbf{v}, \theta_m))) \tag{16a}$$

$$\text{s.t.} \quad \log_2(1 + \kappa_m \cdot \text{Tr}(\mathbf{R}_D \mathbf{A}(\mathbf{v}, \theta_m))) \geqslant S_{\min}, \forall m \tag{16b}$$

$$\log_2 \det\left(\mathbf{I} + \frac{1}{\sigma_c^2} \mathbf{H}_{\text{eff}} \mathbf{R}_D \mathbf{H}_{\text{eff}}^H\right) \geqslant \Gamma_{\min} \tag{16c}$$

$$\text{Tr}(\mathbf{R}_D) = P_{\text{total}}, \quad \mathbf{R}_D \succeq 0 \tag{16d}$$

where $\kappa_m = \beta_m / \sigma_s^2$ denotes the effective SNR scaling coefficient for the m-th monitoring point, mapping the received signal power to the sensing signal-to-noise ratio. This is a convex optimization problem and the solving method is similar to Sub-problem 1.

Sub-problem 2 (Optimizing Passive Beamforming $\mathbf{v}$) : For fixed $\mathbf{R}_D$, the optimization over $\mathbf{v}$ is again non-convex. It can be tackled using SDR in a manner similar to Sub-problem 2 of the first design. The objective function and constraints are transformed into quadratic forms of $\mathbf{v}$, then linearized by lifting to the matrix variable $\mathbf{V}$, and finally solved as an SDP after relaxing the rank-one constraint.

3.2.2 *Algorithm and Complexity Analysis*

The AO algorithm structure is identical to Algorithm 1, but the objective and constraints within the SDP solvers are different.

Algorithm 2 Alternating Optimization for Max-SIR ISAC Design

Initialize:
Channel Matrices $\{\mathbf{H}_{vr}, \mathbf{H}_{vi}, \mathbf{H}_{ir}\}$, Weights $\{w_m\}$,
QoS $\{S_{\min}, \Gamma_{\min}\}$, Power P_{total}, Tolerance ϵ, $K_{\max}$.

$k \leftarrow 0$, $O^{(0)} \leftarrow -\infty$.
Generate $\mathbf{v}^{(0)}$ such that $|v_n^{(0)}| = 1, \forall n$.
Predict and discretize AoI into $\mathcal{S}_{\text{AoI}}$.
repeat
  Step 1: Update Active Beamforming $\mathbf{R}_D$
  Solve the convex problem (16) with fixed $\mathbf{v} \leftarrow \mathbf{v}^{(k)}$ to obtain $\mathbf{R}_D^{(k+1)}$.
  Step 2: Update Passive Beamforming $\mathbf{v}$
  Solve the non-convex problem for $\mathbf{v}$ with fixed $\mathbf{R}_D \leftarrow \mathbf{R}_D^{(k+1)}$ via SDR to obtain $\mathbf{v}^{(k+1)}$.
  Step 3: Update and Check for Convergence
  Calculate the objective value
  $O^{(k+1)} = \sum_{m=1}^{M} w_m R_{\text{sense}}(\mathbf{R}_D^{(k+1)}, \mathbf{v}^{(k+1)}, \theta_m)$.
  $k \leftarrow k + 1$.
until $|O^{(k)} - O^{(k-1)}| \leqslant \epsilon$ **or** $k \geqslant K_{\max}$.
return $\mathbf{R}_D^* \leftarrow \mathbf{R}_D^{(k)}$ and $\mathbf{v}^* \leftarrow \mathbf{v}^{(k)}$.

The computational complexity of Algorithm 2 follows a structure identical to that of the Max-Min SNR design, as it also relies on solving two SDPs within each AO iteration. Let I'_{AO} be the number of iterations for convergence.

- **Sub-problem 1 (Optimizing $\mathbf{R}_D$):** The complexity of solving the convex problem for the $N_t \times N_t$ active covariance matrix remains approximately $\mathcal{O}(MN_t^3)$, determined by the number of transmit antennas N_t and monitoring points M.
- **Sub-problem 2 (Optimizing $\mathbf{v}$ via SDR):** Similarly, the complexity of solving SDR for the passive beamforming is dominated by the number of RIS elements N, scaling as $\mathcal{O}(N^4)$.

Consequently, the overall complexity of Algorithm 2 is also given by $\mathcal{O}\left(I'_{AO} \cdot \left(MN_t^3 + N^4\right)\right)$.

While we utilize established mathematical tools such as AO and Semidefinite Relaxation SDR to handle the non-convex constraints, the core novelty of our approach lies in the sensing-centric objective formulations. By explicitly maximizing the worst-case sensing performance across a dynamically predicted spatial boundary (AoI), rather than optimizing for average throughput, our design inherently caters to the stringent safety requirements of vehicular networks.

4 Simulation Results and Analysis

In this section, we provide extensive numerical results to validate the effectiveness and superiority of our proposed sensing-centric beamforming designs for the RIS-assisted vehicular ISAC system. We first detail the simulation environment, then analyze the convergence of our algorithms, and finally, conduct a comprehensive performance evaluation through a series of eight distinct experiments, comparing our proposals against several state-of-the-art and baseline schemes.

4.1 Simulation Setup

We consider a typical urban canyon scenario as illustrated in Fig. 1. A vehicle (Tx), an RIS, and an RSU (Rx) are located in a 2D coordinate system. The vehicle, located at $(0, 0)$, employs a ULA with $N_t = 16$ antennas. The RIS, with $N = 64$ elements, is positioned at $(50, 20)$ m, and the RSU, with $N_r = 4$ antennas, is at $(100, 10)$ m. The vehicle's behavior-aware AoI is discretized into $M = 10$ monitoring points within an angular sector of $[-30°, 30°]$ and a range of $[20, 80]$ m. All key parameters are summarized in Table 1. Results are averaged over 500 independent channel realizations.

Table 1 Simulation Parameters

Parameter	Value
Carrier Frequency	28 GHz
System Bandwidth	100 MHz
Total Transmit Power, P_{total}	30 dBm (1 W)
Noise Power Spectral Density	-174 dBm/Hz
Noise Figure	5 dB
Number of Tx Antennas, N_t	16
Number of RIS Elements, N	64
Number of Rx Antennas, N_r	4
Number of Data Streams, N_s	2
Path Loss Exponent, α (V-R, V-I)	2.2 (LoS)
Path Loss Exponent, α (I-R)	2.5 (LoS)
Path Loss Exponent, α (Sensing)	2.8 (NLoS-like)
AoI Angular Sector, $[\theta_{\min}, \theta_{\max}]$	$[-30°, 30°]$
AoI Range Sector, $[r_{\min}, r_{\max}]$	$[20, 80]$ meters
Min. Communication Rate, $\Gamma_{\min}$	2 bits/s/Hz
Min. Sensing Rate, $S_{\min}$ (for Max-SIR)	1 bit/s/Hz
AO Convergence Tolerance, ϵ	10^{-4}

4.2 Convergence and Baseline Schemes

We first verify the convergence of the proposed AO-based algorithms. Fig. 5 plots the objective values—minimum sensing SNR for the "Max-Min-SNR" design and total weighted SIR for the "Max-SIR" design—versus the number of AO iterations. As observed, both algorithms demonstrate excellent convergence properties. For instance, the minimum sensing SNR of the Max-Min-SNR algorithm reaches over 95% of its final converged value of 15.86 dB within just 5 iterations. This rapid convergence confirms the efficiency of our proposed iterative solutions, making them viable for dynamic vehicular environments.

To comprehensively evaluate the performance of our two schemes, we compare them against a carefully selected set of five baseline schemes.

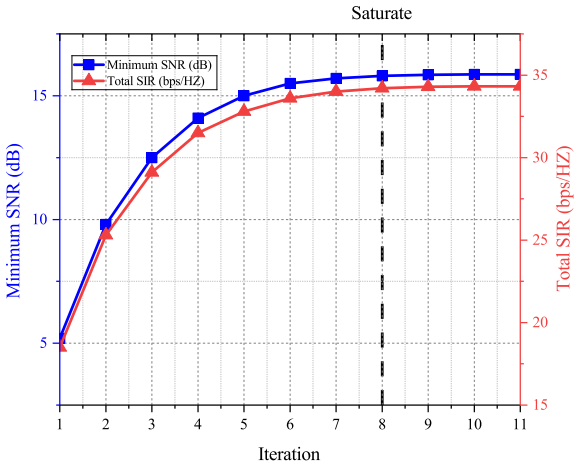

Fig. 5 Convergence behavior performances of two proposed algorithms.

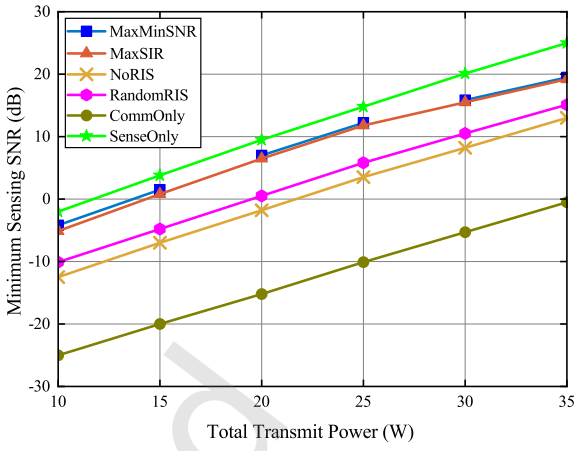

Fig. 6 Impact of transmit power on the minimum sensing SNR.

1. **No RIS:** Optimizes only the active beamforming in a system where the RIS is absent, quantifying the fundamental performance gain of introducing an RIS.

2. **Random Phase RIS:** Optimizes the active beamforming while keeping the RIS phases randomly fixed, isolating the performance gain of intelligent RIS phase control over a simple reflector.

3. **Decoupled Optimization:** Follows a suboptimal two-stage approach by first optimizing the RIS for communication only and then optimizing the active beamforming for the ISAC task.

4. **Communication-Centric Optimization:** Maximizing the communication rate while treating the sensing performance as a minimum quality-of-service constraint.

$$\max_{\mathbf{R}_D,\mathbf{v}} R_{\text{comm}}(\mathbf{R}_D,\mathbf{v})$$
$$\text{s.t.} \quad \text{SNR}_{\text{sense}}(\mathbf{R}_D,\mathbf{v},\theta_m) \geqslant \text{SNR}_{\text{th}}, \forall m$$

5. **Weighted Sum Optimization:** Maximizing a weighted sum of the communication and sensing performance metrics.

$$\max_{\mathbf{R}_D,\mathbf{v}} \quad w\frac{R_{\text{comm}}}{\Gamma_{\text{norm}}} + (1-w)\frac{\sum_m R_{\text{sense}}}{S_{\text{norm}}}$$

where $w \in [0,1]$ is a weighting factor , and $\Gamma_{\text{norm}}, S_{\text{norm}}$ are normalization constants.

6. **Sensing-Only:** Provides a theoretical upper bound on sensing performance by removing the communication QoS constraint and dedicating all system resources to the sensing objective.

To comprehensively evaluate the performance of our two schemes, we compare them against a carefully selected set of baselines. Notably, the 'Decoupled Optimization' and 'Communication-Centric Optimization' baselines represent the standard state-of-the-art (SToA) approaches predominantly utilized in recent ISAC literature, allowing for a direct comparison between prevailing communication-first paradigms and our proposed safety-driven sensing-first philosophy.

4.3 Performance Evaluation and Discussion

In this subsection, we conduct a comprehensive performance analysis across eight distinct experiments. We evaluate both of our proposed schemes, "Max-Min-SNR" and "Max-SIR" and compare them against the suite of baseline schemes.

4.3.1 Experiment 1: Impact of Transmit Power

Fig. 6 illustrates the minimum sensing SNR as a function of the total transmit power. As expected, performance improves for all schemes with increasing power. At $P_{\text{total}} = 30$ dBm, our "Max-Min-SNR" scheme achieves a minimum SNR of 15.86 dB, establishing its superiority in robust coverage. The "Max-SIR" design, while optimizing for total information rate, also achieves a strong minimum SNR of 15.5 dB, significantly outperforming the baselines. Specifically, the "Max-Min-SNR" design shows a remarkable gain of 7.66 dB (a 5.8-fold increase in linear scale) over the "No RIS" scheme (8.2 dB). This highlights that both proposed joint optimization frameworks effectively leverage the available power.

4.3.2 Experiment 2: Impact of Number of RIS Elements

The passive beamforming gain is quantified in Fig. 7. The performance of both "Max-Min-SNR" and "Max-SIR" scales effectively with the number of RIS elements, N. As N increases from 16 to 256, the minimum SNR of the "Max-Min-SNR" design improves from 10.5 dB to 21.0 dB. The

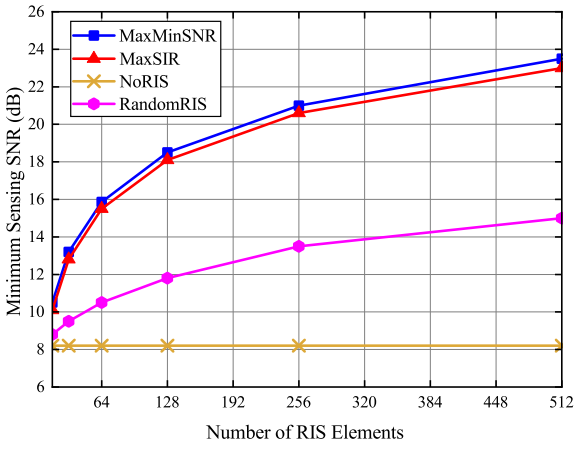

Fig. 7 Impact of number of RIS elements on the minimun sensing SNR.

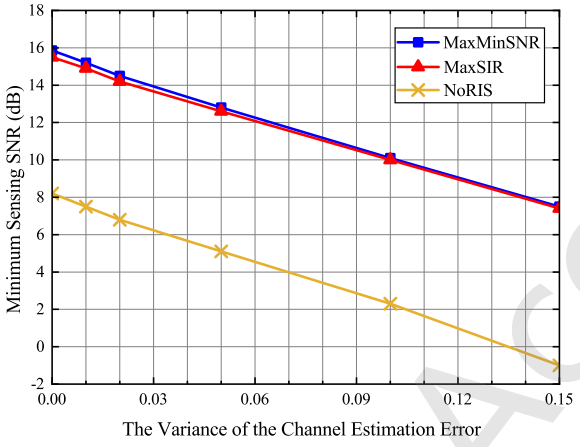

Fig. 8 Robustness analysis against CSI estimation error.

"Max-SIR" design follows a similar trend, improving from 10.1 dB to 20.6 dB. Both proposed designs significantly outperform the "Random Phase RIS" scheme, whose gain saturates quickly. For instance, at $N = 256$, our "Max-Min-SNR" design provides a 7.5 dB advantage over the random phase approach (13.5 dB), confirming the critical importance of intelligent phase control.

4.3.3 *Experiment 3: Robustness to CSI Errors*

Fig. 8 evaluates performance under imperfect CSI. With a channel estimation error variance σ_e^2 of 0.1, the "Max-Min-SNR" and "Max-SIR" designs achieve minimum SNRs of 10.1 dB and 10.0 dB, respectively. While this is a degradation from the perfect CSI case (15.86 dB), they still maintain a significant performance margin of approximately 7.8 dB over the "No RIS" baseline (2.3 dB) under the same error conditions. This demonstrates that our joint optimization frameworks are robust and can provide reliable sensing even when channel knowledge is imperfect.

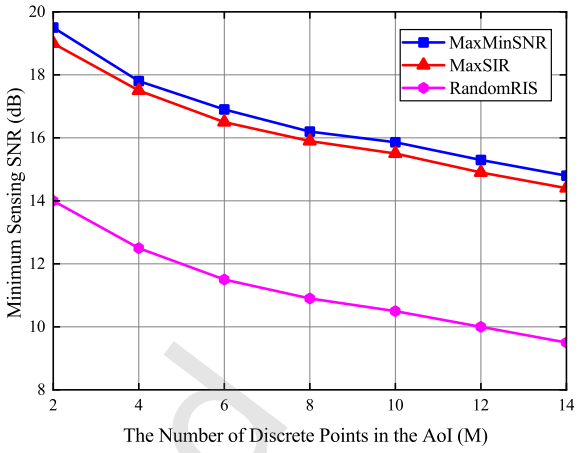

Fig. 9 Performance vs. number of sensing targets (monitoring points M).

4.3.4 *Experiment 4: Performance in Multi-Target Scenarios*

Fig. 9 assesses scalability with an increasing number of sensing targets M. As M increases from 2 to 10, the "Max-Min-SNR" design's performance degrades gracefully from 19.5 dB to 15.86 dB, maintaining its focus on the worst-case target. The "Max-SIR" design degrades slightly faster, from 19.0 dB to 15.5 dB, as its sum-rate objective becomes harder to optimize with more constraints. Both, however, are vastly superior to the "Random Phase RIS" baseline, which drops to 10.5 dB at $M = 10$. This shows our algorithms' superior capability in managing spatial resource allocation in complex scenes.

4.3.5 *Experiment 5: Comparison of Rate-SNR Regions with Baselines*

Fig. 10 provides the most crucial comparison of the achievable performance boundaries. The curves for both "Max-Min-SNR" and "Max-SIR" envelop all other baseline schemes, demonstrating their overall superiority. To guarantee a stringent minimum sensing SNR of 13 dB, our "Max-Min-SNR" design supports a communication rate of 3.5 bps/s/Hz. The "Max-SIR" design is very competitive, achieving 3.4 bps/s/Hz for the same sensing quality. In contrast, the "Decoupled Opt." scheme supports only 2.2 bps/s/Hz, which is over 37% lower in communication throughput. This starkly illustrates the substantial performance loss from non-joint optimization.

4.3.6 *Experiment 6: Beampattern Uniformity Analysis with Baselines*

Fig. 11 visualizes the generated sensing beampatterns. As designed, the beampattern for "Max-Min-SNR" is exceptionally flat across the AoI of $[-30°, 30°]$, with a power variation of only 0.6 dB. This confirms its success in robust coverage. The "Max-SIR" beampattern also concentrates energy effectively

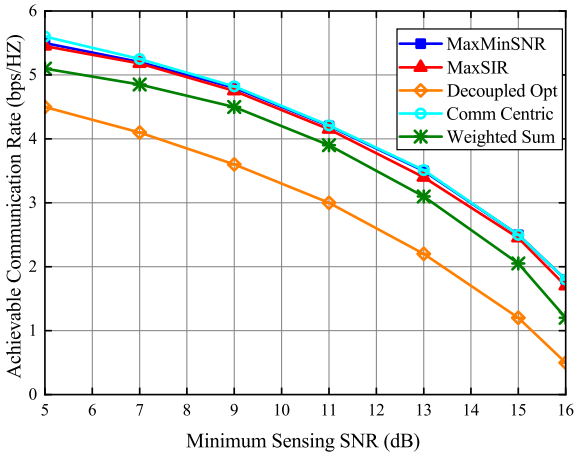

Fig. 10 Rate-SNR region comparison of different algorithms.

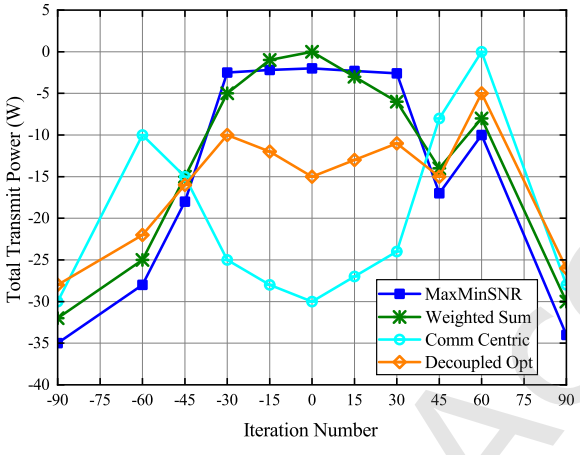

Fig. 11 Sensing beampattern comparison of different algorithms.

within the AoI but with more variation (a 4 dB dip at the edges compared to the center), as its goal is to maximize the total rate, not uniformity. In stark contrast, the "Comm-Centric" scheme focuses its main lobe at 60° (the RSU's direction), resulting in an SNR in the AoI that is more than 25 dB lower than our proposed designs. This provides compelling visual proof of the different strategies and the effectiveness of our sensing-centric philosophy.

5 Conclusion

In this paper, we have developed and analyzed two novel, sensing-centric frameworks for the joint design of active and passive beamforming in an RIS-assisted vehicular ISAC system. We proposed two distinct algorithms: a robust Max-Min-SNR design focused on uniform safety coverage, and an information-theoretic Max-SIR design focused on maximizing overall environmental information acquisition. To solve the challenging non-convex problems, we developed efficient iterative algorithms based on alternating optimization and semidefinite relaxation. Our extensive simulation results have compellingly demonstrated the superiority of both proposed algorithms. The Max-Min-SNR algorithm, true to its design, provides exceptionally uniform sensing coverage and achieves a remarkable 7.66 dB improvement in worst-case sensing SNR compared to a non-RIS system. For a given stringent sensing requirement, it can support up to a 59% higher communication rate than a traditional decoupled optimization strategy. The Max-SIR algorithm also proved highly effective, establishing its value as a powerful alternative. It successfully maximizes the perceptual information gain, achieving a total sensing information rate that is 45% higher than the conventional weighted sum optimization approach. Furthermore, both designs proved robust against CSI errors and practical hardware limitations.Future work will focus on integrating predictive beamforming and real-time channel tracking techniques to further mitigate the performance degradation caused by outdated CSI in ultra-high-speed scenarios. While the proposed AO and SDR based algorithms establish valuable theoretical performance upper bounds and validate the effectiveness of the sensing-centric philosophy, their high computational complexity ($\mathcal{O}(N^4)$) poses challenges for real-time deployment in vehicular networks. To address this, future research will explore the integration of low-complexity, real-time algorithms—such as Deep Reinforcement Learning (DRL) or heuristic gradient-based methods—to translate these robust designs into practically deployable solutions. Furthermore, extending the current single-vehicle model to a complex multi-vehicle scenario represents a critical future direction. In realistic urban environments, multiple ISAC vehicles will inevitably generate inter-vehicle interference (IVI). Addressing this will require advanced coordinated multi-agent beamforming frameworks, where the optimization problem must incorporate spatial nulling constraints to suppress interference toward adjacent vehicles, alongside orthogonal time-frequency resource allocation schemes to ensure cooperative coexistence.

Reference

[1] M. Banafaa, I. Shayea, J. Din, M. H. Azmi, A. Alashbi, Y. I. Daradkeh, and A. Alhammadi, 6G mobile communication technology: Requirements, targets, applications, challenges, advantages, and opportunities, *Alexandria Eng. J.*, vol. 64, pp. 245–274, Feb. 2023.

[2] C.-X. Wang, X. You, X. Gao, X. Zhu, Z. Li, C. Zhang, H. Wang, Y. Huang, Y. Chen, H. Haas *et al.*, On the road to 6G: Visions, requirements, key technologies and testbeds, *IEEE Commun. Surveys Tuts.*, vol. 25, no. 2, pp. 905–974, 2nd Quart. 2023.

[3] Z. Zhang, Y. Xiao, Z. Ma, M. Xiao, Z. Ding, X. Lei, G. K. Karagiannidis, and P. Fan, 6G wireless networks: Vision,

requirements, architecture, and key technologies, *IEEE Veh. Technol. Mag.*, vol. 14, no. 3, pp. 28–41, Jul. 2019.

[4] B. Li, S. Li, A. Nallanathan, and C. Zhao, Deep sensing for future spectrum and location awareness 5G communications, *IEEE J. Sel. Areas Commun.*, vol. 33, no. 7, pp. 1331–1344, Jul. 2015.

[5] C. Xu, K. Xu, L. Feng, and B. Liang, RetroV2X: A new vehicle-to-everything (V2X) paradigm with visible light backscatter networking, *Fundamental Research*, vol. 5, no. 3, pp. 1204–1213, May. 2025.

[6] S. Gyawali, S. Xu, Y. Qian, and R. Q. Hu, Challenges and solutions for cellular based V2X communications, *IEEE Commun. Surveys Tuts.*, vol. 23, no. 1, pp. 222–255, 1st Quart. 2021.

[7] C. R. Storck and F. Duarte-Figueiredo, A survey of 5G technology evolution, standards, and infrastructure associated with vehicle-to-everything communications by Internet of vehicles, *IEEE Access*, vol. 8, pp. 117 593–117 614, Jun. 2020.

[8] P. Agbaje, A. Anjum, A. Mitra, E. Oseghale, G. Bloom, and H. Olufowobi, Survey of interoperability challenges in the Internet of vehicles, *IEEE Trans. Intell. Transp. Syst.*, vol. 23, no. 12, pp. 22 838–22 861, Dec. 2022.

[9] M. Stoyanova, Y. Nikoloudakis, S. Panagiotakis, E. Pallis, and E. K. Markakis, A survey on the Internet of things (IoT) forensics: Challenges, approaches, and open issues, *IEEE Commun. Surveys Tuts.*, vol. 22, no. 2, pp. 1191–1221, 2nd Quart. 2020.

[10] J. Xu, C. Yuen, C. Huang, N. Ul Hassan, G. C. Alexandropoulos, M. Di Renzo, and M. Debbah, Reconfiguring wireless environments via intelligent surfaces for 6G: Reflection, modulation, and security, *Sci. China. Inf. Sci.*, vol. 66, no. 3, p. 130304, Feb. 2023.

[11] X. Li, Y. Gong, K. Huang, and Z. Niu, Over-the-air integrated sensing, communication, and computation in IoT networks, *IEEE Wireless Commun.*, vol. 30, no. 1, pp. 32–38, Feb. 2023.

[12] Y. Huang, Challenges and opportunities of sub-6 GHz integrated sensing and communications for 5G-advanced and beyond, *Chinese J. Electron.*, vol. 33, no. 2, pp. 323–325, Mar. 2024.

[13] D. Wang, C. Huang, J. He, C. Zhu, W. Wang, X. Chen, Z. Zhang, Z. Han, and M. Debbah, Waveform precoding design for mobile crowd ISCC system using mean field game, in *Proc. IEEE Globecom WKSHPS. (GC Wkshps)*, Dec. 2023.

[14] Y. Xu, T. Zhang, Y. Liu, and D. Yang, UAV-enabled integrated sensing, computing, and communication: A fundamental trade-off, *IEEE Wireless Commun. Lett.*, vol. 12, no. 5, pp. 843–847, May 2023.

[15] W. Liu, Z. Jin, X. Zhang, W. Zang, S. Wang, and Y. Shen, AoI-aware UAV-enabled marine MEC networks with integrated sensing, computation, and communication, in *Proc. IEEE/CIC Int. Conf. Commun. in China (ICCC Wkshps)*, Aug. 2023.

[16] Z. Wei, H. Liu, X. Yang, W. Jiang, H. Wu, X. Li, and Z. Feng, Carrier aggregation enabled integrated sensing and communication signal design and processing, *IEEE Trans. Veh. Technol.*, vol. 73, no. 3, pp. 3580–3596, Oct. 2023.

[17] N. H. Chu, D. N. Nguyen, D. T. Hoang, Q.-V. Pham, K. T. Phan, W.-J. Hwang, and E. Dutkiewicz, AI-enabled mm-waveform configuration for autonomous vehicles with integrated communication and sensing, *IEEE Internet Things J.*, vol. 10, no. 19, pp. 16 727–16 743, Oct. 2023.

[18] K. P. Rajput, L. Wu, and M. R. Bhavani Shankar, Next-generation IoT networks: Integrated sensing communication and computation, in *Proc. IEEE Int. Conf. Acoustics, Speech, Signal Process. WKSHPS. (ICASSPW)*, Jun. 2023.

[19] E. Moradi-Pari, D. Tian, M. Bahramgiri, S. Rajab, and S. Bai, DSRC versus LTE-V2X: Empirical performance analysis of direct vehicular communication technologies, *IEEE Trans. Intell. Transp. Syst.*, vol. 24, no. 5, pp. 4889–4903, May 2023.

[20] J. Hu, Z. Chen, and J. Luo, Multi-band reconfigurable holographic surface based ISAC systems: Design and optimization, in *Proc. IEEE Int. Conf. Commun. (ICC)*, Jun. 2023.

[21] D. Cong, S. Guo, S. Dang, and H. Zhang, Vehicular behavior-aware beamforming design for integrated sensing and communication systems, *IEEE Trans. Intell. Transp. Syst.*, vol. 24, no. 6, pp. 5923–5935, Jun. 2023.

[22] H. Wang, L. Wan, M. Dong, K. Ota, and X. Wang, Assistant vehicle localization based on three collaborative base stations via sbl-based robust doa estimation, *IEEE Internet of Things Journal*, vol. 6, no. 3, pp. 5766–5777, 2019.

[23] X. Wang, L. T. Yang, D. Meng, M. Dong, K. Ota, and H. Wang, Multi-uav cooperative localization for marine targets based on weighted subspace fitting in sagin environment, *IEEE Internet of Things Journal*, vol. 9, no. 8, pp. 5708–5718, 2022.

[24] F. Zhu, X. Wang, C. Huang, Z. Yang, X. Chen, A. Alhammadi, Z. Zhang, C. Yuen, and M. Debbah, Robust beamforming for RIS-aided communications: Gradient-based manifold meta learning, *IEEE Trans. Wireless Commun.*, pp. 1–1, Aug. 2024.

[25] F. Zhu, X. Wang, C. Huang, A. Alhammadi, H. Chen, Z. Zhang, C. Yuen, and M. Debbah, Beamforming inferring by conditional wgan-gp for holographic antenna arrays, *IEEE Wireless Commun. Lett.*, vol. 13, no. 7, pp. 2023–2027, Jul. 2024.

[26] R. Liu, M. Li, H. Luo, Q. Liu, and A. L. Swindlehurst, Integrated sensing and communication with reconfigurable intelligent surfaces: Opportunities, applications, and future directions, *IEEE Wireless Commun.*, vol. 30, no. 1, pp. 50–57, Feb. 2023.

[27] Z. Gao, X. Zhou, B. Ning, Y. Su, T. Qin, and D. Niyato, Integrated location sensing and communication for ultra-massive mimo with hybrid-field beam-squint effect, *IEEE J. Sel. Areas Commun.*, vol. 43, no. 4, pp. 1387–1404, Feb. 2025.

[28] Z. Gao, Z. Wan, D. Zheng, S. Tan, C. Masouros, D. W. K. Ng, and S. Chen, Integrated sensing and communication with mmwave massive mimo: A compressed sampling perspective, *IEEE Trans. Wireless Commun.*, vol. 22, no. 3, pp. 1745–1762, Sep. 2023.

[29] C. Huang, A. Zappone, G. C. Alexandropoulos, M. Debbah,

and C. Yuen, Reconfigurable intelligent surfaces for energy efficiency in wireless communication, *IEEE Trans. Wireless Commun.*, vol. 18, no. 8, pp. 4157–4170, Aug. 2019.

[30] Z. Zhang and L. Dai, Reconfigurable intelligent surfaces for 6G: Nine fundamental issues and one critical problem, *Tsinghua Sci. Technol.*, vol. 28, no. 5, pp. 929–939, 2023.

[31] B. Ning, Z. Chen, W. Chen, and J. Fang, Beamforming optimization for intelligent reflecting surface assisted MIMO: A sum-path-gain maximization approach, *IEEE Wireless Commun. Lett.*, vol. 9, no. 7, pp. 1105–1109, Mar. 2020.

[32] B. Ning, Z. Chen, Z. Tian, X. Wang, C. Pan, J. Fang, and S. Li, Joint power allocation and passive beamforming design for IRS-assisted physical-layer service integration, *IEEE Tran. Wireless Commun.*, vol. 20, no. 11, pp. 7286–7301, May 2021.

[33] B. Ning, P. Wang, L. Li, Z. Chen, and J. Fang, Multi-IRS-aided multi-user MIMO in mmWave/THz communications: A space-orthogonal scheme, *IEEE Trans. Commun.*, vol. 70, no. 12, pp. 8138–8152, Dec. 2022.

[34] M. I. Ismail, A. M. Shaheen, M. M. Fouda, and A. S. Alwakeel, RIS-assisted integrated sensing and communication systems: Joint reflection and beamforming design, *IEEE Open J. Commun. Soc.*, vol. 5, pp. 908–927, Jan. 2024.

[35] G. Zhou, C. Pan, H. Ren, P. Popovski, and A. L. Swindlehurst, Channel estimation for RIS-aided multiuser millimeter-wave systems, *IEEE Trans. Signal Process.*, vol. 70, pp. 1478–1492, Mar. 2022.

[36] C. Huang, S. Hu, G. C. Alexandropoulos, A. Zappone, C. Yuen, R. Zhang, M. Di Renzo, and M. Debbah, Holographic mimo surfaces for 6G wireless networks: Opportunities, challenges, and trends, *IEEE Wireless Commun.*, vol. 27, no. 5, pp. 118–125, Oct. 2020.

[37] Q. Zhu, M. Li, R. Liu, and Q. Liu, Joint transceiver beamforming and reflecting design for active RIS-aided ISAC systems, *IEEE Trans. Veh. Technol.*, vol. 25, no. 6, pp. 5554–5566, Jul. 2023.

[38] P. Saikia, S. Pala, K. Singh, S. K. Singh, and W.-J. Huang, Proximal policy optimization for RIS-assisted full duplex 6G-V2X communications, *IEEE Transa. Intell. Veh.*, pp. 1–16, May 2023.

[39] X. Gan, C. Huang, Z. Yang, C. Zhong, X. Chen, Z. Zhang, Q. Guo, C. Yuen, and M. Debbah, Bayesian learning for double-RIS aided ISAC systems with superimposed pilots and data, *IEEE J. Sel. Topics Signal Process*, pp. 1–16, May 2024.

[40] Z. Wang, Y. Zhou, Y. Zou, Q. An, Y. Shi, and M. Bennis, A graph neural network learning approach to optimize RIS-assisted federated learning, *IEEE Trans. Wireless Commun.*, vol. 22, no. 9, pp. 6092–6106, Sep. 2023.

[41] Z. Chen, P. Chen, Z. Guo, Y. Zhang, and X. Wang, A ris-based vehicle DOA estimation method with integrated sensing and communication system, *IEEE Trans. Intell. Transp. Syst.*, vol. 25, no. 6, pp. 5554–5566, Jun. 2024.

[42] Z. Zhu, M. Gong, G. Sun, P. Liu, and D. Mi, AI-enabled STAR-RIS aided MISO ISAC secure communications, *Tsinghua Sci. Technol.*, vol. 30, no. 3, pp. 998–1011, 2025.

[43] X. Wang, Z. Fei, J. Huang, and H. Yu, Joint waveform and discrete phase shift design for RIS-assisted integrated sensing and communication system under Cramer-Rao bound constraint, *IEEE Trans. Veh. Technol.*, vol. 71, no. 1, pp. 1004–1009, Jan. 2022.

[44] S. P. Chepuri, N. Shlezinger, F. Liu, G. C. Alexandropoulos, S. Buzzi, and Y. C. Eldar, Integrated sensing and communications with reconfigurable intelligent surfaces: From signal modeling to processing, *IEEE Signal Process. Mag.*, vol. 40, no. 6, pp. 41–62, Sep. 2023.

[45] D. Wang, W. Wang, Z. Zhang, and A. Huang, Delay-optimal random access in large-scale energy harvesting IoT networks based on mean field game, *China Commun.*, vol. 19, no. 4, pp. 121–136, Apr. 2022.

[46] L. Zhao, D. Wu, L. Zhou, and Y. Qian, Radio resource allocation for integrated sensing, communication, and computation networks, *IEEE Trans. Wireless Commun.*, vol. 21, no. 10, pp. 8675–8687, Oct. 2022.

[47] P. Liu, G. Zhu, S. Wang, W. Jiang, W. Luo, H. V. Poor, and S. Cui, Toward ambient intelligence: Federated edge learning with task-oriented sensing, computation, and communication integration, *IEEE J. Sel. Topics Signal Process.*, vol. 17, no. 1, pp. 158–172, Jan. 2023.

[48] B. Li, W. Liu, W. Xie, N. Zhang, and Y. Zhang, Adaptive digital twin for UAV-assisted integrated sensing, communication, and computation networks, *IEEE Trans. Green Commun. Netw.*, vol. 7, no. 4, pp. 1996–2009, Dec. 2023.

[49] J. Zou, C. Wang, Y. Liu, Z. Zou, and S. Sun, Vision-assisted 3-D predictive beamforming for green UAV-to-vehicle communications, *IEEE Trans. Green Commun. Netw.*, vol. 7, no. 1, pp. 434–443, Mar. 2023.

[50] N. Huang, C. Dou, Y. Wu, L. Qian, B. Lin, and H. Zhou, Unmanned-aerial-vehicle-aided integrated sensing and computation with mobile-edge computing, *IEEE Internet Things J.*, vol. 10, no. 19, pp. 16 830–16 844, Oct. 2023.

[51] X. Meng, F. Liu, C. Masouros, W. Yuan, Q. Zhang, and Z. Feng, Vehicular connectivity on complex trajectories: Roadway-geometry aware ISAC beam-tracking, *IEEE Trans. Wireless Commun.*, vol. 22, no. 11, pp. 7408–7423, Nov. 2023.

[52] Z. Yu, H. Ren, C. Pan, G. Zhou, B. Wang, M. Dong, and J. Wang, Active RIS-aided ISAC systems: Beamforming design and performance analysis, *IEEE Trans. Commun.*, vol. 72, no. 3, pp. 1578–1595, Mar. 2024.

[53] B. Zheng, C. You, W. Mei, and R. Zhang, A survey on channel estimation and practical passive beamforming design for intelligent reflecting surface aided wireless communications, *IEEE Commun. Surveys Tuts.*, vol. 24, no. 2, pp. 1035–1071, 2022.

[54] M. Grant and S. Boyd, CVX: Matlab software for disciplined convex programming, version 2.1, Jan. 2014.

[55] Z.-q. Luo, W.-k. Ma, A. M.-c. So, Y. Ye, and S. Zhang,

Semidefinite relaxation of quadratic optimization problems, *IEEE Signal Process. Mag.*, vol. 27, no. 3, pp. 20–34, 2010.

Author biography

Ruihang Yang received the B.S. degree in communication engineering from Hohai University, Nanjing, China, in 2017, the M.Sc. degree from Southwest University, Chongqing, China, in 2021. He is currently pursuing the Ph.D. degree with College of Information Science and Electronic Engineering, Zhejiang University. His research interests include 6G wireless communication, integrated sensing and computing, intelligent reflecting surface, and convex optimization.

Li Wei received the B.Sc. degree in communication engineering from Southwest Jiaotong University, China, in 2015, the M.Sc. degree in electronic and communication engineering from Xidian University, China, in 2019, and the Ph.D. degree from Singapore University of Technology and Design, Singapore, in 2023. She is currently a Research Fellow with the School of Electrical and Electronic Engineering, Nanyang Technological University, Singapore. Her research interests include holographic MIMO communications, reconfigurable intelligent surfaces, and electromagnetic information theory.

Chongwen Huang obtained his B. Sc. degree in 2010 from Nankai University, and the M.Sc degree from the University of Electronic Science and Technology of China in 2013, and PhD degree from Singapore University of Technology and Design (SUTD) in 2019. From Oct. 2019 to Sep. 2020, he is a Postdoc in SUTD. Since Sep. 2020, he joined into Zhejiang University as a tenure-track young professor. Dr. Huang is the recipient of 2021 IEEE Marconi Prize Paper Award, 2023 IEEE Fred W. Ellersick Prize Paper Award and 2021 IEEE ComSoc Asia-Pacific Outstanding Young Researcher Award. He has served as an Editor of IEEE Communications Letter, Elsevier Signal Processing, EURASIP Journal on Wireless Communications and Networking and Physical Communication since 2021. His main research interests are focused on Holographic MIMO Surface/Reconfigurable Intelligent Surface, B5G/6G Wireless Communications, mmWave/THz Communications, Deep Learning technologies for Wireless communications, etc.